Critical phenomena of asymmetric nuclear matter in the extended Zimanyi-Moszkowski model

K. Miyazaki*

Abstract

We have studied the liquid-gas phase transition of warm asymmetric nuclear matter in the extended Zimanyi-Moszkowski model. The three sets of the isovector-meson coupling constants are used. It is found that the critical temperature depends only on the difference of the symmetry energy but not on the differences of each isovector coupling constant. We treat the asymmetric nuclear matter as one-component system and employ the Maxwell construction so as to calculate the liquid-gas phase coexistence curve. The derived critical exponents depend on neither the symmetry energy nor the asymmetry of the system. Their values $\beta = 0.33$ and $\gamma = 1.21$ agree with the empirical values derived from the recent multifragmentation reactions. Consequently, we have confirmed the universality of the critical phenomena in the liquid-gas phase transition of nuclear matter.

1 Introduction

Now, it is well known [1,2] that the nuclear equation-of-state (EOS) behaves like van der Waals EOS and so shows liquid-gas phase transition. In the resent progress of nuclear multifragmentation reaction, the signals of the phase transition are observed in the plateau of the caloric curves [3] and the negative heat capacity [4]. The critical temperature T_C of the phase transition is also derived in several experimental efforts [5,6]. Although their values depend on the methods of analyses and are scattered over the wide range due to the Coulomb interaction and the finite-size effect, Natowitz *et al.* [7] have succeeded to estimate the critical temperature for infinite symmetric nuclear matter, that is, $T_C = 16.6 \pm 0.86\,\mathrm{MeV}$.

Unfortunately, most of theoretical EOSs cannot reproduce this empirical value of T_C. To the contrary, in the recent work [8] the author has shown that the extended Zimanyi-Moszkowski model [9,10] of relativistic mean-field theory [11] for nuclear matter can reproduce the value. Moreover, the model reproduces the critical exponents β and γ derived from multifragmentation reactions [6,12-14], which also agree with their universal values for liquid-gas phase transition of various materials. It is however noted that the

*E-mail : miyazakiro@rio.odn.ne.jp

hot homogeneous nuclear matter produced by heavy-ion reactions is isospin asymmetric. Although the critical exponents are expected to be universal and so do not depend on the asymmetry, we have to confirm the universality. Therefore in the present work we will extend the investigation of ref. [8] to asymmetric nuclear matter.

2 Formalism

The EZM model for asymmetric nuclear matter at finite temperature has already been developed in Ref. [15]. Nevertheless, for the completeness and convenience, we represent the formulation here. The thermodynamic potential per volume $\tilde{\Omega} \equiv \Omega/V$ of asymmetric nuclear matter at temperature T is

$$\begin{aligned}\tilde{\Omega} &= \frac{1}{2}\, m_\sigma^2 \langle\sigma\rangle^2 + \frac{1}{2}\, m_\delta^2 \langle\delta_3\rangle^2 - \frac{1}{2}\, m_\omega^2 \langle\omega_0\rangle^2 - \frac{1}{2}\, m_\rho^2 \langle\rho_{03}\rangle^2 \\ &\quad - \gamma\, k_B T \sum_{i=p,n} \int_0^\infty \frac{d^3\mathbf{k}}{(2\pi)^3} \left\{ \ln\left[1+\exp\left(\frac{\nu_i - E_{ki}^*}{k_B T}\right)\right] + \ln\left[1+\exp\left(\frac{-\nu_i - E_{ki}^*}{k_B T}\right)\right] \right\},\end{aligned} \tag{1}$$

where k_B is the Boltzmann constant and $E_{ki}^* = (\mathbf{k}^2 + M_i^{*2})^{1/2}$ with the effective mass M_i^* of a proton or neutron in the medium. The spin degeneracy factor γ is equal to 2. The ν_i is defined by the chemical potential μ_i and the vector potential V_{0i} of a proton or neutron as

$$\nu_i = \mu_i - V_{0i}. \tag{2}$$

The isoscalar scalar mean-field $\langle\sigma\rangle$ is determined from the effective masses by

$$\langle\sigma\rangle = \frac{\left(1-m_p^*\right) g_{nn\delta}^* + \left(1-m_n^*\right) g_{pp\delta}^*}{g_{pp\sigma}^* g_{nn\delta}^* + g_{nn\sigma}^* g_{pp\delta}^*} M, \tag{3}$$

where M is the free nucleon mass and $M_i^* = m_i^* M$. Similarly, the isovector scalar mean-field $\langle\delta_3\rangle$ is determined by

$$\langle\delta_3\rangle = \frac{\left(1-m_p^*\right) g_{nn\sigma}^* - \left(1-m_n^*\right) g_{pp\sigma}^*}{g_{pp\sigma}^* g_{nn\delta}^* + g_{nn\sigma}^* g_{pp\delta}^*} M. \tag{4}$$

On the other hand, the isoscalar vector mean-field $\langle\omega_0\rangle$ is determined from the vector potentials as

$$\langle\omega_0\rangle = \frac{g_{nn\rho}^* v_{0p} + g_{pp\rho}^* v_{0n}}{g_{pp\omega}^* g_{nn\rho}^* + g_{nn\omega}^* g_{pp\rho}^*} M, \tag{5}$$

where $V_{0i} = v_{0i} M$. Similarly, the isovector vector mean-field $\langle \rho_{03} \rangle$ is determined from

$$\langle \rho_{03} \rangle = \frac{g^*_{nn\omega} v_{0p} - g^*_{pp\omega} v_{0n}}{g^*_{pp\omega} g^*_{nn\rho} + g^*_{nn\omega} g^*_{pp\rho}} M. \tag{6}$$

The renormalized meson coupling constants [10] are

$$g^*_{pp(nn)\Pi} = h^*_{pp(nn)\Pi}\, g_{NN\Pi} \quad (\Pi = \sigma,\ \omega,\ \delta,\ \rho)\,, \tag{7}$$

$$h^*_{pp\sigma(\omega)} = (1-\lambda) + \lambda\, m^*_p, \tag{8}$$

$$h^*_{nn\sigma(\omega)} = (1-\lambda) + \lambda\, m^*_n. \tag{9}$$

$$h^*_{pp\delta(\rho)} = (1-\lambda) + \lambda \left(2m^*_n - m^*_p\right), \tag{10}$$

$$h^*_{nn\delta(\rho)} = (1-\lambda) + \lambda \left(2m^*_p - m^*_n\right), \tag{11}$$

with

$$\lambda = 1/3. \tag{12}$$

It is noted that $\lambda = 0$ corresponds to the Walecka model [11].

Then the effective mass m^*_i and the vector potential v_{0i} are determined from extremizing the thermodynamical potential $\tilde{\Omega}$ by them. The results are

$$\frac{\rho_{Bp}}{M} - \left(\frac{m_\omega}{g_{NN\omega}}\right)^2 \frac{\left(h^*_{nn\rho} v_{0p} + h^*_{pp\rho} v_{0n}\right) h^*_{nn\rho}}{D^2} - \left(\frac{m_\rho}{g_{NN\rho}}\right)^2 \frac{\left(h^*_{nn\omega} v_{0p} - h^*_{pp\omega} v_{0n}\right) h^*_{nn\omega}}{D^2} = 0, \tag{13}$$

$$\frac{\rho_{Bn}}{M} - \left(\frac{m_\omega}{g_{NN\omega}}\right)^2 \frac{\left(h^*_{nn\rho} v_{0p} + h^*_{pp\rho} v_{0n}\right) h^*_{pp\rho}}{D^2} + \left(\frac{m_\rho}{g_{NN\rho}}\right)^2 \frac{\left(h^*_{nn\omega} v_{0p} - h^*_{pp\omega} v_{0n}\right) h^*_{pp\omega}}{D^2} = 0, \tag{14}$$

$$\begin{aligned}
&\frac{\rho_{Sp}}{M} + \left(\frac{m_\sigma}{g_{NN\sigma}}\right)^2 \frac{A^{(0)}\left(A^{(1)}_p C^{(0)} - A^{(0)} C^{(1)}_p\right)}{\left(C^{(0)}\right)^3} + \left(\frac{m_\delta}{g_{NN\delta}}\right)^2 \frac{B^{(0)}\left(C^{(0)} - B^{(0)} C^{(1)}_p\right)}{\left(C^{(0)}\right)^3} \\
&+ \lambda \left(\frac{m_\omega}{g_{NN\omega}}\right)^2 \frac{h^*_{nn\rho} v_{0p} + h^*_{pp\rho} v_{0n}}{D^3} \left[\left({h^*_{nn\rho}}^2 - 2h^*_{nn\omega} h^*_{pp\rho} - h^*_{nn\omega} h^*_{nn\rho}\right) v_{0p}\right. \\
&\qquad \left. + \left(h^*_{pp\omega} h^*_{nn\rho} + h^*_{pp\rho} h^*_{nn\rho} + 2h^*_{pp\omega} h^*_{pp\rho}\right) v_{0n}\right] \\
&+ \lambda \left(\frac{m_\rho}{g_{NN\rho}}\right)^2 \frac{h^*_{nn\omega} v_{0p} - h^*_{pp\omega} v_{0n}}{D^3} \left[h^*_{nn\omega}\left(h^*_{nn\rho} + 2h^*_{pp\omega} - h^*_{nn\omega}\right) v_{0p}\right. \\
&\qquad \left. + \left(h^*_{nn\omega} h^*_{pp\rho} - 2{h^*_{pp\omega}}^2 + h^*_{pp\omega} h^*_{nn\omega}\right) v_{0n}\right] = 0,
\end{aligned} \tag{15}$$

$$\frac{\rho_{Sn}}{M}+\left(\frac{m_\sigma}{g_{NN\sigma}}\right)^2\frac{A^{(0)}\left(A_n^{(1)}C^{(0)}-A^{(0)}C_n^{(1)}\right)}{\left(C^{(0)}\right)^3}-\left(\frac{m_\delta}{g_{NN\delta}}\right)^2\frac{B^{(0)}\left(C^{(0)}+B^{(0)}C_n^{(1)}\right)}{\left(C^{(0)}\right)^3}$$
$$+\lambda\left(\frac{m_\omega}{g_{NN\omega}}\right)^2\frac{h^*_{nn\rho}v_{0p}+h^*_{pp\rho}v_{0n}}{D^3}\left[\left(h^*_{nn\rho}h^*_{nn\omega}+2h^*_{nn\omega}h^*_{nn\rho}+h^*_{pp\rho}h^*_{nn\rho}\right)v_{0p}\right.$$
$$\left.+\left({h^*_{pp\rho}}^2-h^*_{pp\omega}h^*_{pp\rho}-2h^*_{pp\omega}h^*_{nn\rho}\right)v_{0n}\right]$$
$$+\lambda\left(\frac{m_\rho}{g_{NN\rho}}\right)^2\frac{h^*_{nn\omega}v_{0p}-h^*_{pp\omega}v_{0n}}{D^3}\left[\left(2{h^*_{nn\omega}}^2-h^*_{pp\omega}h^*_{nn\omega}-h^*_{pp\omega}h^*_{nn\rho}\right)v_{0p}\right.$$
$$\left.+h^*_{pp\omega}\left(h^*_{pp\omega}-h^*_{pp\rho}-2h^*_{nn\omega}\right)v_{0n}\right]=0, \tag{16}$$

where the quantities A, B, C and D are defined by

$$A^{(0)}=h^*_{nn\delta}\left(m^*_p-1\right)+h^*_{pp\delta}\left(m^*_n-1\right), \tag{17}$$

$$B^{(0)}=h^*_{nn\sigma}\left(m^*_p-1\right)-h^*_{pp\sigma}\left(m^*_n-1\right), \tag{18}$$

$$C^{(0)}=h^*_{pp\sigma}h^*_{nn\delta}+h^*_{nn\sigma}h^*_{pp\delta}, \tag{19}$$

$$A_p^{(1)}=(1-\xi)+\xi\left(2m^*_p-m^*_n\right), \tag{20}$$

$$C_p^{(1)}=\xi\,h^*_{nn\delta}, \tag{21}$$

$$A_n^{(1)}=(1-\xi)+\xi\left(2m^*_n-m^*_p\right), \tag{22}$$

$$C_n^{(1)}=\xi\,h^*_{pp\delta}, \tag{23}$$

$$D=h^*_{pp\omega}h^*_{nn\rho}+h^*_{nn\omega}h^*_{pp\rho} \tag{24}$$

with $\xi\equiv 2\lambda$.

The baryon and scalar densities are defined by

$$\rho_{Bi}=\gamma\int_0^\infty\frac{d^3\mathbf{k}}{(2\pi)^3}\left[n_{ki}(T)-\bar{n}_{ki}(T)\right], \tag{25}$$

$$\rho_{Si}=\gamma\int_0^\infty\frac{d^3\mathbf{k}}{(2\pi)^3}\frac{M^*_i}{E^*_{ki}}\left[n_{ki}(T)+\bar{n}_{ki}(T)\right]. \tag{26}$$

The Fermi-Dirac distribution functions of nucleon and antinucleon are

$$n_{ki}(T)=\left[1+\exp\left(\frac{E^*_{ki}-\nu_i}{k_BT}\right)\right]^{-1}, \tag{27}$$

$$\bar{n}_{ki}(T)=\left[1+\exp\left(\frac{E^*_{ki}+\nu_i}{k_BT}\right)\right]^{-1}. \tag{28}$$

The energy density is given by

$$\begin{aligned}\mathcal{E} &= \gamma \sum_{i=p,n} \int_0^\infty \frac{d^3\mathbf{k}}{(2\pi)^3} E^*_{ki} \left[n_{ki}(T) + \bar{n}_{ki}(T) \right] \\ &+ \frac{1}{2}\left(\frac{m_\sigma M}{g_{NN\sigma}}\right)^2 \left(\frac{A^{(0)}}{C^{(0)}}\right)^2 + \frac{1}{2}\left(\frac{m_\delta M}{g_{NN\delta}}\right)^2 \left(\frac{B^{(0)}}{C^{(0)}}\right)^2 \\ &+ \frac{1}{2}\left(\frac{g_{NN\omega}}{m_\omega}\right)^2 \left(h^*_{pp\omega}\rho_{Bp} + h^*_{nn\omega}\rho_{Bn}\right)^2 + \frac{1}{2}\left(\frac{g_{NN\rho}}{m_\rho}\right)^2 \left(h^*_{pp\rho}\rho_{Bp} - h^*_{nn\rho}\rho_{Bn}\right)^2, \end{aligned} \tag{29}$$

and the pressure is

$$P = -\tilde{\Omega}. \tag{30}$$

3 Numerical analyses

Given the total baryon density $\rho_B = \rho_{Bn} + \rho_{Bp}$, the asymmetry $a = \left(\rho_{Bn} - \rho_{Bp}\right)/\rho_B$ and the temperature T, Eqs. (13)-(16) and (25) have to be solved numerically utilizing 6-dimensional Newton-Raphson method so that the effective masses m^*_p and m^*_n, the vector potentials v_{0p} and v_{0n}, and the chemical potentials μ_p and μ_n are determined selfconsistently.

Employing the isoscalar-meson coupling constants in Ref. [9] and the isovector-meson coupling constants $\left(g_{NN\delta}/m_\delta\right)^2 = 0.39\,\mathrm{fm}^2$ and $\left(g_{NN\rho}/m_\rho\right)^2 = 0.82\,\mathrm{fm}^2$ (hereafter referred to as the coupling set 1) from Bonn A potential [16], Figs. 1-4 calculate the pressure-density isotherms for $a = 0.2$, 0.4, 0.6 and 0.8, respectively. We clearly see the behaviors like van der Waals EOS and the liquid-gas phase transitions. The critical temperatures (T_C), and the pressures (P_C) and the baryon densities (ρ_C) at inflection points are summarized in Table 1. Moreover, the flash temperatures, above which the pressure is always positive at any finite density, are T =12.451, 11.245, 9.275 and 6.559 MeV, respectively. The solid curve in Fig. 5 shows the dependence of T_C on the asymmetry. The decrease of T_C with increasing asymmetry is the common feature to other models [17-20].

The isovector-meson coupling set 1 predicts lower symmetry energy $E_s = 24.6\,\mathrm{MeV}$ than its empirical value $30 \pm 4\,\mathrm{MeV}$. This is due to the relatively weak $NN\rho$ coupling. In order to investigate the effect of the symmetry energy, we also calculate using another coupling set 2 in which the $NN\delta$ coupling is the same as set 1 but the $NN\rho$ coupling $\left(g_{NN\rho}/m_\rho\right)^2 = 1.432\,\mathrm{fm}^2$ is stronger so that the symmetry energy $E_s = 32.0\,\mathrm{MeV}$ is reproduced. Moreover, in order to investigate the effect of ambiguity in the isovector coupling constants, we calculate using the coupling set 3 that also reproduces $E_s = 32.0\,\mathrm{MeV}$, but has stronger $NN\delta$ coupling $\left(g_{NN\delta}/m_\delta\right)^2 = 1.0\,\mathrm{fm}^2$ and much stronger $NN\rho$ coupling $\left(g_{NN\rho}/m_\rho\right)^2 = 1.888\,\mathrm{fm}^2$. The critical temperatures and the inflection points using the set 2 and 3 are summarized in Table 2 and 3, respectively. The dependences

of T_C on the asymmetry are also shown by the dotted and dashed curves in Fig. 5, respectively.

In the comparison of the solid curve with the dotted one in Fig. 5, it is seen that the difference of the symmetry energy has large effect on the critical temperature especially at high asymmetry. On the contrary, in the comparison of the dotted curve with the dashed one, we see that the differences in each isovector coupling constant have little effect on the temperature under definite symmetry energy. The most conspicuous difference due to the symmetry energy is that the solid curve has the value $T_C = 4.973\,\mathrm{MeV}$ even at $a = 1.0$ while the dotted and dashed curves vanish above $a = 0.941$ and $a = 0.960$, respectively. In other words, for the lower symmetry energy we can always see the liquid-gas phase transition while for the higher symmetry energy there are critical asymmetries, above which no liquid-gas phase transitions occur. Such a critical asymmetry has also been reported in Refs. [18] and [20]. Although they did not investigate the effect of the symmetry energy, we can guess their results are also due to the higher symmetry energies than $E_s = 32.0\,\mathrm{MeV}$.

Then we will investigate the critical phenomena of asymmetric nuclear matter. Here it is noted that the asymmetric nuclear matter is usually treated as two-component system [21]. Namely, the proton and neutron are independent components because their chemical potentials are different from each other due to the isovector-meson mean-fields. However in this case we do not have the phase coexistence curve in temperature-density plain but the phase boundary (or separation) curve. See the curve marked with "CE" on Fig. 22(a) in Ref. [21]. On the curve the liquid and gas phases at a definite temperature do not coexist because their pressures are different from each other. (See also Fig. 4 in Ref. [21].) Moreover, the maximum temperature of the phase boundary curve does not agree with the critical point. This situation is not consistent to the analyses [6,22] in multifragmentation reactions.

For the comparison with the experimental analyses, in the present work the asymmetric nuclear matter is treated as one-component system. Namely, we consider only the Gibbs energy per particle $\tilde{G} = \left(\rho_{Bp}\mu_p + \rho_{Bn}\mu_n\right)/\rho_B$ rather than each chemical potential. The phase coexistence curve is determined by the Maxwell construction. The results are shown in Fig. 6. The black solid and dotted curves are calculated for $a = 0.2$ using the isovector-meson coupling set 1 and 2, respectively. The result for the coupling set 3 has not been calculated because it is essentially the same as the set 2 as seen in Fig. 5. We can see that there is little difference between the two curves because their densities and asymmetries are relatively low. Although the asymmetry higher than $a = 0.2$ has no physical correspondence in the present multifragmentation experiments, in order to show the effect of the asymmetry we also calculate the red solid curve for $a = 0.4$ using the coupling set 1. The difference between the results of $a = 0.2$ and $a = 0.4$ is apparent.

Then the critical exponents β and γ will be investigated. Figure 7 shows the difference between the densities of the nuclear liquid (ρ_l) and gas $\left(\rho_g\right)$ phases versus tem-

perature in log scale. The circles are calculated on the black solid curve in Fig. 6 at $T = 6.0, 7.0 \cdots 15.0, 15.2 \cdots 15.8\,\mathrm{MeV}$ while the crosses are the results using the coupling set 2 from $T = 6.0\,\mathrm{MeV}$ to $T = 15.6\,\mathrm{MeV}$. In the near region to the critical point the results lie on the red line while in the far region from the critical point they lie on the blue line. The warm asymmetric nuclear matter clearly exhibits the critical phenomenon that does not depend on the symmetry energy. The inclination of the line is just the critical exponent β. According to its theoretical definition it seems reasonable to derive the value $\beta = 0.48 \simeq 1/2$. It is however noted that in heavy-ion reactions the limit of Coulomb instability prevents the nuclear system from reaching the critical point [22] and so the empirical value of β is derived in the far region from the critical point [14]. According to this fact, Fig. 7 predicts $\beta = 0.33 \simeq 1/3$ from the blue line rather than $\beta = 0.48 \simeq 1/2$ from the red line. The value agrees well with those derived from multifragmentation reactions [6,12-14] and the universal value of the liquid-gas phase transition.

Figure 8 shows the inverse of incompressibility κ versus temperature in log scale:

$$\frac{1}{\kappa} \propto \frac{\rho_B}{P_C}\frac{\partial P}{\partial \rho_B} \propto \left(1 - \frac{T}{T_C}\right)^{\gamma}. \tag{31}$$

The circles and crosses are calculated on the liquid branches of the phase coexistence curves for $a = 0.2$ in Fig. 6 at the same temperatures as Fig. 7. In contrast to Fig. 7 the results lie on the single blue line. The obtained critical exponent $\gamma = 1.21$ also agrees with the empirical value derived from multifragmentation reactions [13-15] and the universal value of the liquid-gas phase transition.

We have already calculated the critical exponents for symmetric nuclear matter in Ref. [8]. In fact, the nuclear system produced by heavy-ion reaction is isospin asymmetric. Therefore the present calculations for asymmetric nuclear matter seem to be more reasonable for the comparison with experiments. Nevertheless, the above results of the critical exponents in Figs. 7 and 8 are in good agreement with the results of Ref. [8]. This suggests that the critical phenomena does not depend on the asymmetry and so is universal. In order to confirm the universality, we further investigate the critical exponents for $a = 0.4$ although such a large asymmetry has not been realized in the present experiments of multifragmentation reactions. Figure 9 is the same as Fig. 7, but the circles are calculated on the red solid curve in Fig. 6 at $T = 5.0, 6.0 \cdots 14.0, 14.2, 14.4\,\mathrm{MeV}$. They lie on the red and blue lines again in the near region to and the far region from the critical point, respectively. Figure 10 is the same as Fig. 8, but the circles are calculated on the liquid branch of the red curve in Fig. 6 at the same temperatures as Fig. 9. They lie on the single blue line as in Fig. 8. Because only the β derived from the blue line in Fig. 9 is slightly smaller than that in Fig. 7, we can assert that the critical exponents do not depend on the asymmetry.

4 Summary

We have studied the thermodynamics of warm asymmetric nuclear matter below the saturation density in the EZM model. The EOS behaves like van der Waals one and so clearly shows the liquid-gas phase transition. The critical temperature decreases as the asymmetry of the system increases. We have investigated three sets of the isovector coupling constants. The first one is from Bonn A potential but predicts relatively lower symmetry energy than its empirical value. The second one has much stronger $NN\rho$ coupling than the first so as to reproduce the empirical symmetry energy. The third one has much stronger $NN\delta$ coupling than the first and second ones but reproduces the same symmetry energy as the second. It is found that the critical temperature depends only on the difference of the symmetry energy but not the differences of each isovector coupling. Moreover, for the coupling set 2 and 3, we have found the critical asymmetry, above which no liquid-gas phase transitions occur.

For calculating the liquid-gas phase coexistence curve in the pressure-density plain, we treat the asymmetric nuclear matter as one-component system and employ the Maxwell construction. This prescription is consistent to the experimental analyses of multifragmentation reactions. Then the critical exponents β and γ are derived. Their values for the asymmetry $a = 0.2$ do not depend on the symmetry energy, and agree well with the empirical values derived from multifragmentation reactions and the universal values for the liquid-gas phase transition. Moreover, for the symmetric case $a = 0.0$ and for higher asymmetry $a = 0.4$ we find almost the same critical exponents as $a = 0.2$. Consequently, the universality of the critical phenomena in the liquid-gas phase transition of nuclear matter has been confirmed. In a future work we will investigate whether the universality can be extended to strange hadronic matter.

References

[1] J. Richert and P. Wagner, Phys. Rep. **350** (2001) 1, [arXiv:nucl-th/0009023]

[2] S.D. Gupta, A.Z. Mekjian and M.B. Tsang, *Advances in Nuclear Physics*, Vol. **26** (Kluwer Academic, 2001), [arXiv:nucl-th/0009033].

[3] J.B. Natowitz *et al.* Phys. Rev. **C65** (2002) 034618, [arXiv:nucl-ex/0106016].

[4] B. Borderie *et al.* Nucl. Phys. **A734** (2004) 495, [arxiv:nucl-ex/0311016].

[5] V.A. Karnaukhov *et al.* Phys. Rev. **C67** (2003) 011601, [arXiv:nucl-ex/0302006].

[6] J.B. Elliott *et al.* Phys. Rev. **C67** (2003) 024609, [arXiv:nucl-ex/0205004].

[7] J.B. Natowitz *et al.* Phys. Rev. Lett. **89** (2002) 212701, [arXiv:nucl-ex/0204015].

[8] K. Miyazaki, Mathematical Physics Preprint Archive (mp_arc) 05-261.

[9] K. Miyazaki, Mathematical Physics Preprint Archive (mp_arc) 05-178

[10] K. Miyazaki, Mathematical Physics Preprint Archive (mp_arc) 05-190.

[11] B.D. Serot and J.D. Walecka, *Advances in Nuclear Physics*, Vol. **16** (Plenum, New York, 1986).

[12] B.K. Srivastava *et al.* Phys. Rev. **C65** (2002) 054617, [arXiv:nucl-ex/0202023].

[13] D. Kudzia, B. Wilczyńska and H. Wilczyński, Phys. Rev. **C68** (2003) 054903, [arXiv:nucl-ex/0207017].

[14] Y.G. Ma *et al.* Phys. Rev. **C71** (2005) 054606, [arXiv:nucl-ex/0410018].

[15] K. Miyazaki, Mathematical Physics Preprint Archive (mp_arc) 05-293.

[16] R. Brockmann and R. Machleidt, Phys. Rev. **C42** (1990) 1965.

[17] H. Huber, F. Weber and M.K. Weigel, Phys. Rev. **C57** (1998) 3484, [arXiv:nucl-th:9803026].

[18] P.K. Panda, G. Krein, D.P. Menezes and C. Providência, Phys. Rev. **C68** (2003) 015201, [arXiv:nucl-th/0306045].

[19] P.K. Sahu, T.K. Jha, K.C. Panda and S.K. Patra, Nucl. Phys. **A733** (2004) 169, [arXiv:nucl-th/0312128].

[20] P. Wang, D.B. Leinweber, A.W. Thomas and A.G. Williams, Nucl. Phys. **A748** (2005) 226, [arXiv:nucl-th/0407057].

[21] H. Müller and B.D. Serot, Phys. Rev. **C52** (1995) 2072, [arXiv:nucl-th/9505013].

[22] J.B. Natowitz *et al.* arXiv:nucl-ex/0206010.

Table 1: The critical temperature T_C, and the pressure P_C and the baryon density ρ_C at inflection point in the pressure-density isotherm for several asymmetries using the isovector-meson coupling set 1.

	$a = 0.0$	$a = 0.2$	$a = 0.4$	$a = 0.6$	$a = 0.8$
T_C (MeV)	16.360	15.906	14.554	12.340	9.261
P_C $\left(\text{MeV/fm}^3\right)$	0.3078	0.2925	0.2492	0.1862	0.1142
ρ_C (fm^{-3})	0.0588	0.0574	0.0533	0.0468	0.0381

Table 2: The same as Table 1 but for the isovector-meson coupling set 2.

	$a = 0.0$	$a = 0.2$	$a = 0.4$	$a = 0.6$	$a = 0.8$
T_C (MeV)	16.360	15.732	13.864	10.790	6.413
P_C $\left(\text{MeV/fm}^3\right)$	0.3078	0.2877	0.2318	0.1522	0.0659
ρ_C (fm^{-3})	0.0588	0.0572	0.0520	0.0437	0.0317

Table 3: The same as Table 1 but for the isovector-meson coupling set 3.

	$a = 0.0$	$a = 0.2$	$a = 0.4$	$a = 0.6$	$a = 0.8$
T_C (MeV)	16.360	15.725	13.855	10.836	6.667
P_C $\left(\text{MeV/fm}^3\right)$	0.3078	0.2869	0.2298	0.1509	0.0681
ρ_C (fm^{-3})	0.0588	0.0570	0.0516	0.0431	0.0315

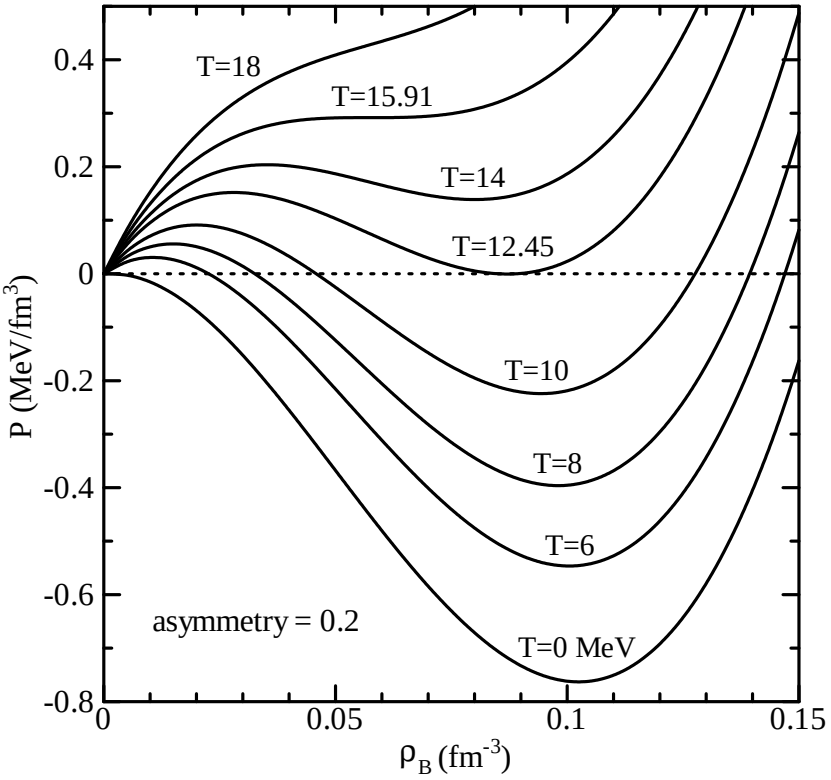

Figure 1: The pressure-density isotherms of asymmetric nuclear matter with $a = 0.2$ using the isovector-meson coupling set 1.

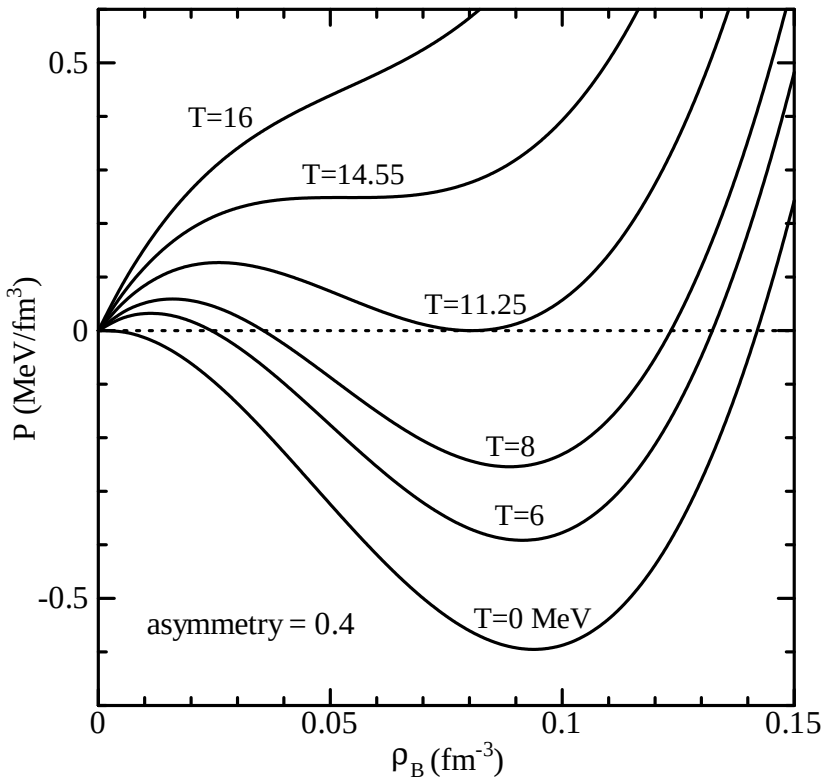

Figure 2: The same as Fig. 1 but for $a = 0.4$.

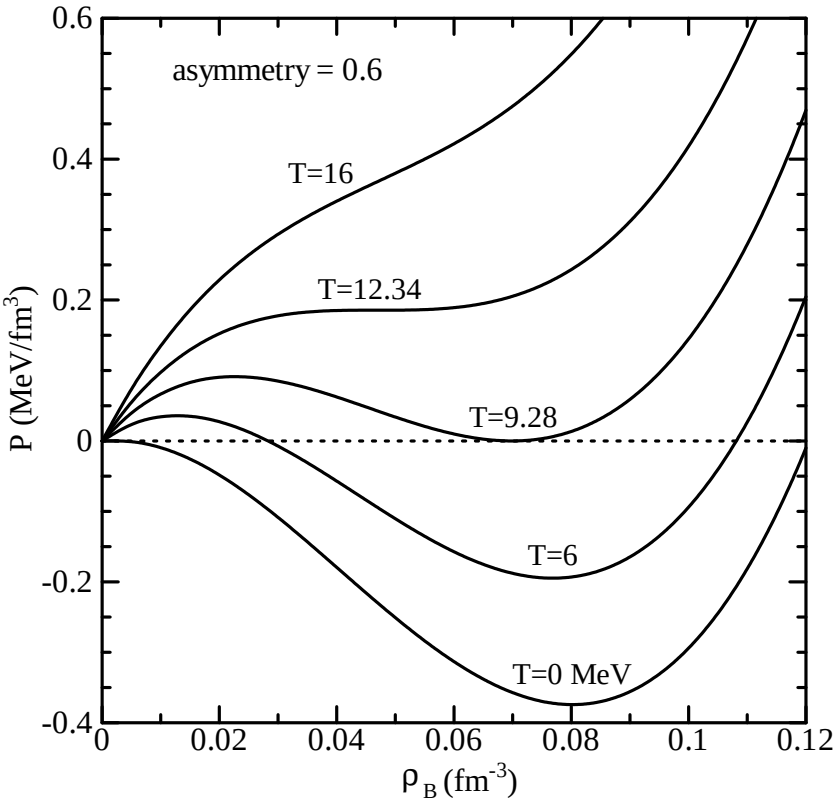

Figure 3: The same as Fig. 1 but for $a = 0.6$.

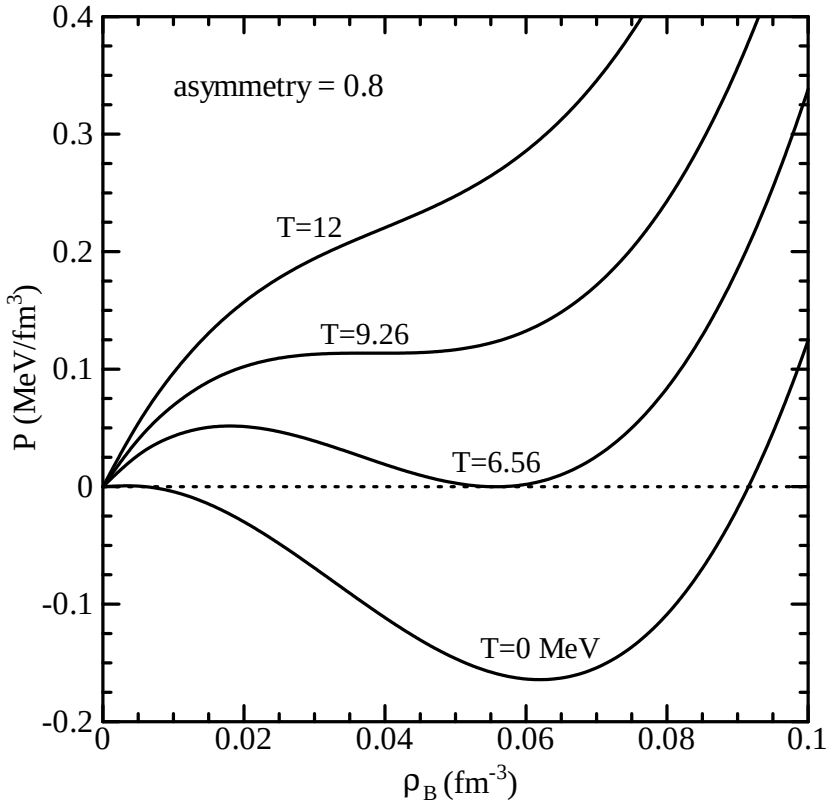

Figure 4: The same as Fig. 1 but for $a = 0.8$.

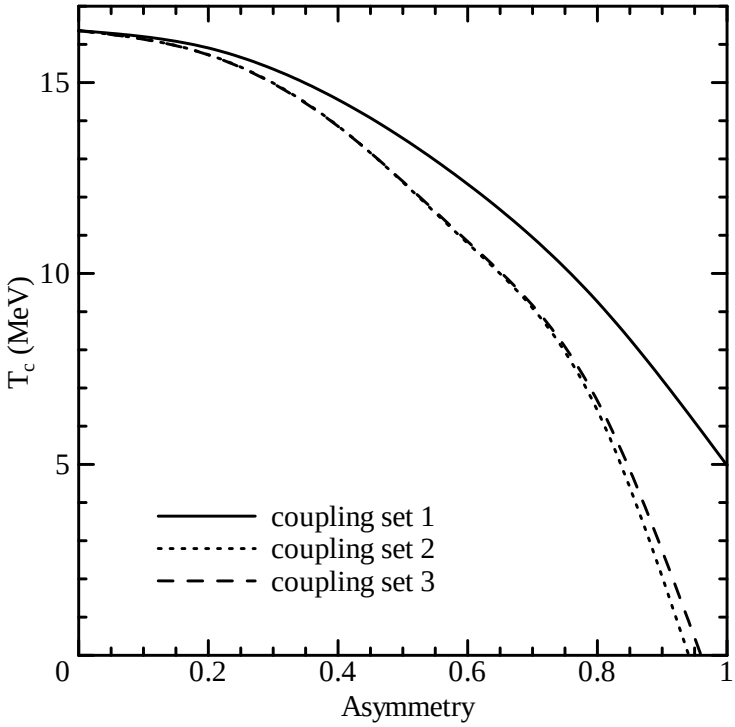

Figure 5: The dependence of the critical temperature on the asymmetry. The solid, dotted and dashed curves are the results using the isovector-meson coupling set 1, 2 and 3, respectively.

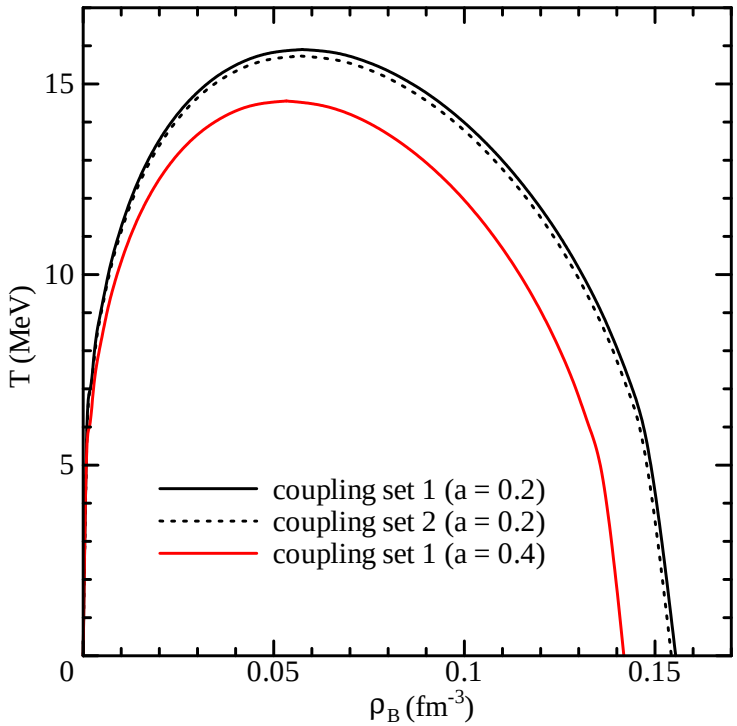

Figure 6: The liquid-gas phase coexistence curves. The black solid and dotted curves are the results for $a = 0.2$ using the isovector-meson coupling set 1 and 2. The red solid curve is the result for $a = 0.4$ using the coupling set 1.

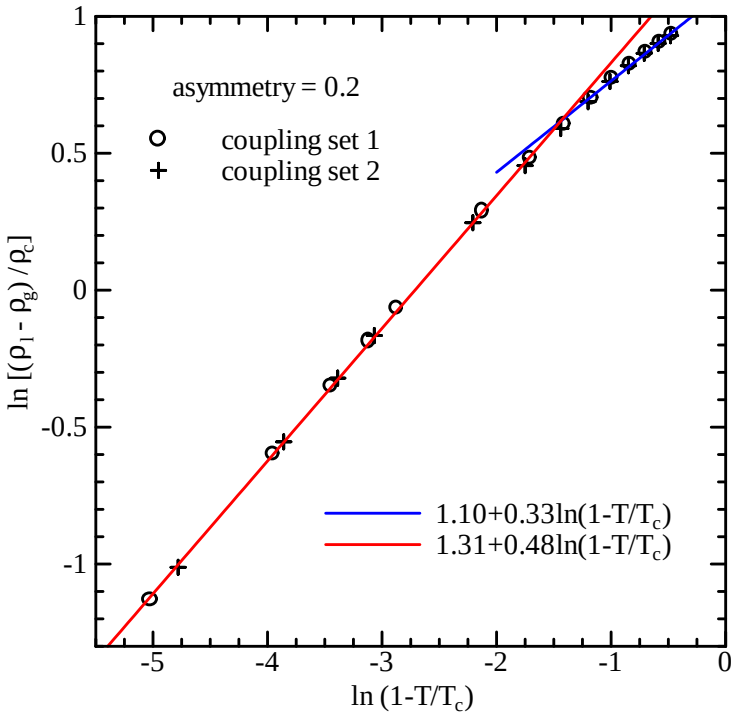

Figure 7: The difference between the densities of the nuclear liquid (ρ_l) and gas (ρ_g) phases versus temperature in log scale calculated on the black solid and dotted curves in Fig. 6.

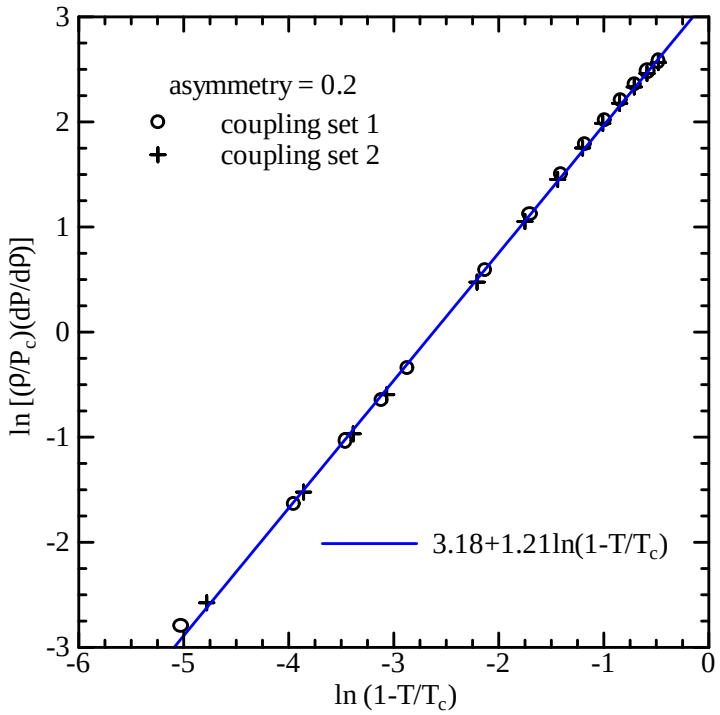

Figure 8: The inverse of compressibility versus temperature in log scale calculated on the liquid branches of the black solid and dotted curves in Fig. 6 at the same temperatures as Fig. 7.

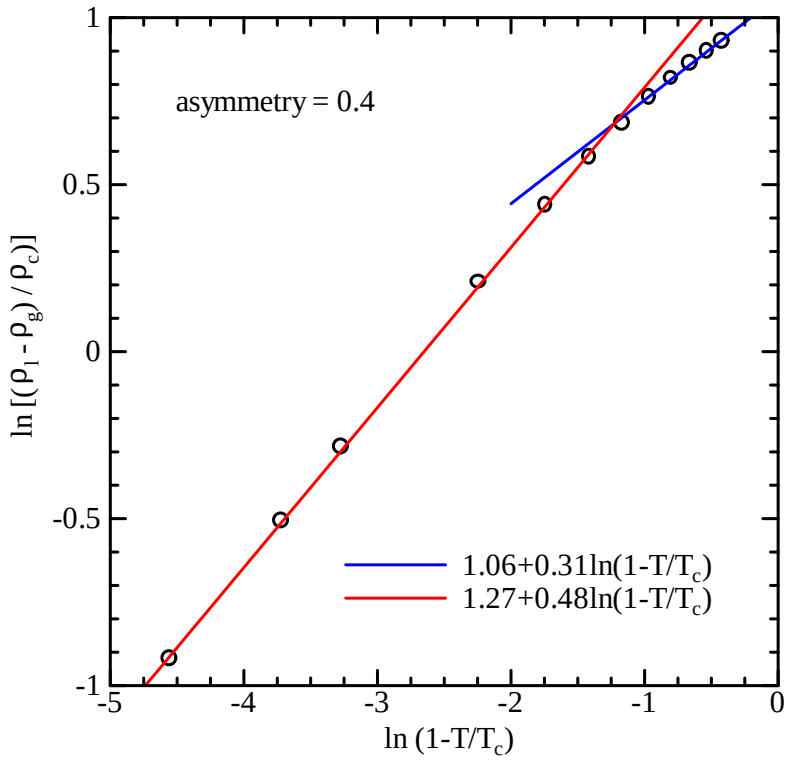

Figure 9: The difference between the densities of the nuclear liquid (ρ_l) and gas (ρ_g) phases versus temperature in log scale calculated on the red solid curve in Fig. 6.

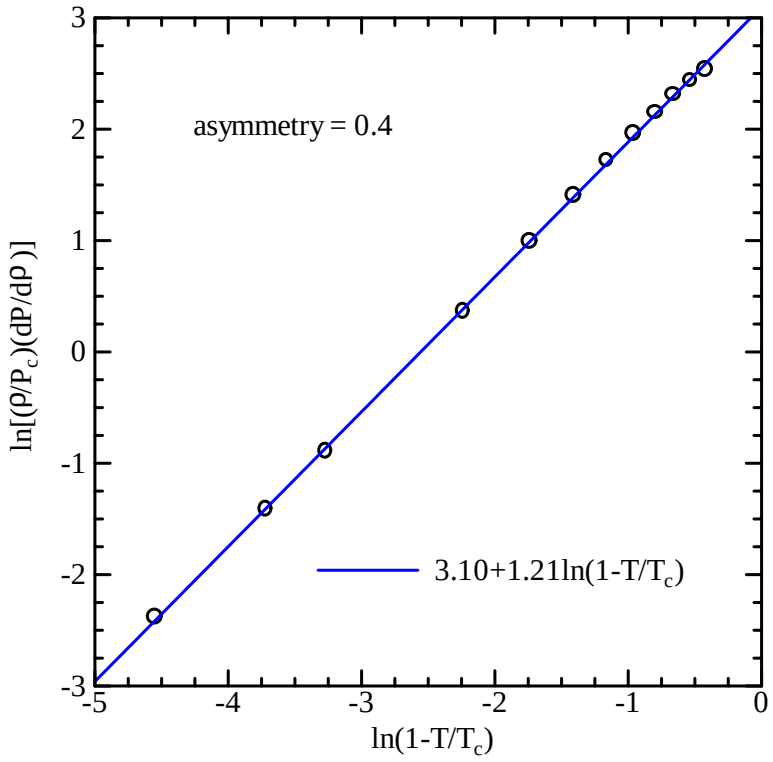

Figure 10: The inverse of compressibility versus temperature in log scale calculated on the liquid branch of the red solid curve in Fig. 6 at the same temperatures as Fig. 9.